Space Weather

RESEARCH ARTICLE
10.1029/2022SW003234

Ensemble Modeling of Radiation Belt Electron Acceleration by Chorus Waves: Dependence on Key Input Parameters

Man Hua[1], Jacob Bortnik[1], Adam C. Kellerman[2], Enrico Camporeale[3], and Qianli Ma[1,4]

[1]Department of Atmospheric and Oceanic Sciences, UCLA, Los Angeles, CA, USA, [2]Department of Earth, Planetary, and Space Sciences, UCLA, Los Angeles, CA, USA, [3]CIRES, University of Colorado Boulder, Boulder, CO, USA, [4]Center for Space Physics, Boston University, Boston, MA, USA

Abstract We perform ensemble simulations of radiation belt electron acceleration using the quasi-linear approach during the storm on 9 October 2012, where chorus waves dominated electron acceleration at $L = 5.2$. Based on a superposed epoch analysis of 11 similar storms when both multi-MeV electron flux enhancements and chorus wave activities were observed by Van Allen Probes, we use percentiles to sample the normalized input distributions for the four key inputs to estimate their relative perturbations. Using 11 points in each input parameter including chorus wave amplitude B_w, chorus wave peak frequency f_m, background magnetic field B_0, and electron density N_e, we ran 11^4 simulations to quantify the impact of uncertainties in the input parameters on the resulting simulated electron acceleration by chorus. By comparing the simulations to observations, our ensemble simulations reveal that inaccuracies in all four input parameters significantly affect the simulated electron acceleration, with the largest simulation errors attributed to the uncertainties in B_w, N_e, and f_m. The simulation can deviate from the observations by four orders of magnitude, while members with largest probability density (smallest perturbations in the input) provide reasonable estimations of output fluxes with log accuracy errors concentrated between ~ -2.0 and 0.5. Quantifying the uncertainties in our study is a prerequisite for the validation of our radiation belt electron model and improvements of accurate electron flux predictions.

Plain Language Summary The ensemble modeling technique has only been embraced by the space weather community for about 20 years and is a powerful numerical method that can help us understand how the uncertainty propagates in the model, as well as the confidence and range of simulated results. Quantifying the error distribution and model performance is important to improve space weather predictions. We perform an ensemble of simulations of radiation belt electron acceleration using the quasi-linear approach during the storm on 9 October 2012, where chorus waves dominated electron acceleration at $L = 5.2$. By conducting a superposed epoch analysis of 11 similar storms when both multi-MeV electron flux enhancements and chorus wave activities were observed, we improve the input data sampling in terms of both spatiotemporal coverage and extreme case coverage. The comparison between the ensemble simulations and observations allows us to quantify how the uncertainties in the simulated output fluxes are apportioned to inaccuracy in the input parameters. We also estimate the confidence of the simulation performance by calculating the probability density of the simulation error. Our sensitive analysis provides fundamental information for radiation belt model calibration and future accurate radiation belt electron predictions.

Key Points:

- We perform ensemble simulations of radiation belt electron acceleration by chorus with input sampling using multi-event observations
- Simulations are strongly affected by uncertainties in all four key inputs, especially by wave amplitude, wave peak frequency, and density
- The ensembles can overestimate acceleration by four orders, while members with largest probability density provide reasonable predictions

Supporting Information:

Supporting Information may be found in the online version of this article.

Correspondence to:

M. Hua,
manhua@ucla.edu

Citation:

Hua, M., Bortnik, J., Kellerman, A. C., Camporeale, E., & Ma, Q. (2023). Ensemble modeling of radiation belt electron acceleration by chorus waves: Dependence on key input parameters. *Space Weather*, *21*, e2022SW003234. https://doi.org/10.1029/2022SW003234

Received 25 JUL 2022
Accepted 9 JAN 2023

1. Introduction

Since the discovery of the Earth's radiation belts in 1958, understanding and forecasting the energetic electron dynamics in this region have been the top concern for space physics community (e.g., Baker, 1998; Ripoll et al., 2020; Summers et al., 2011; W. Li & Hudson, 2019). These energetic electrons pose a hazard to satellites and humans in space, and are also known as "killer" electrons (e.g., Baker, 2001; Baker et al., 1998) due to their deleterious effects. The energetic electrons in the outer radiation belt manifest various acceleration and loss processes (e.g., Baker et al., 2004, 2019; Reeves et al., 2016; Turner et al., 2014), where the magnitude of fluxes can vary by several orders of magnitude within a few hours. It has been well recognized that there are two major sources to accelerate energetic electrons at hundreds of keV to relativistic and ultrarelativistic energies in the outer belt: inward radial diffusion by Ultra-Low Frequency and local-wave particle interactions by whistler-mode chorus waves (e.g., Drozdov et al., 2022, and references therein; Tu et al., 2019; W. Li & Hudson, 2019). Previous studies have demonstrated that electron acceleration is dominated by inward radial diffusion when the radial profile

of the electron phase space density (PSD) exhibit a positive energy gradient during non-storm or storm times, and typically for relatively lower values of the first adiabatic invariant (e.g., Jaynes et al., 2018; Ma et al., 2018; Ozeke et al., 2020; Zhao et al., 2018, 2019). In contrast, chorus waves are primarily responsible for the electron acceleration around the growing peak of the radial profile of electron PSD at the heart of the outer radiation belt (e.g., Horne, 2007; Reeves et al., 2013; Thorne et al., 2013; Turner et al., 2013; W. Li, Ma, et al., 2016). Although numerous studies have demonstrated that nonlinear interactions by chorus waves with large amplitude and coherent structures are potentially important in affecting outer belt electron dynamics (e.g., Albert et al., 2021; Bortnik et al., 2008; Gan et al., 2020; Mourenas et al., 2018; Tao et al., 2012; Zhang et al., 2018), the quasi-linear theory is still the most widely adopted (and possibly the only) approach to reproduce the essential features of observed electron acceleration by chorus on a global scale in terms of space and time on relatively long timescales (from hours to days; e.g., Horne et al., 2005; Hua, Bortnik, & Ma, 2022; Turner et al., 2014; W. Li et al., 2014; Xiao et al., 2014). Most event-based studies construct the simulation model by including the plasma wave model, the background magnetic field model, and the total electron density model based on satellite observations within several days (e.g., C. Wang et al., 2017; Hua et al., 2018; Ma et al., 2015, 2016; Ni et al., 2014, 2017; Ripoll et al., 2016, 2017, 2019; Tu et al., 2014), which can be inaccurate due to the insufficient in-situ satellite measurements with limited spatiotemporal coverage and magnetic local time (MLT) sampling during the event, or due to the instrument limitations. To compound the problem, the quasi-linear simulation strongly depends on the accurate simulation model (e.g., Abel & Thorne, 1998; Agapitov et al., 2019; Albert et al., 2020; Camporeale et al., 2016; Hua, Bortnik, Kellerman, et al., 2022; Hua et al., 2019; Lei et al., 2017). Statistical models remain vital for radiation belt modeling efforts. Watt et al. (2019) and Ross et al. (2020) developed a method to calculate, and average over the diffusion coefficients using simultaneous observations of the individual plasma and wave parameters instead of the averaged values of the input conditions. These two studies suggest an alternative, and potentially improved methodology for creating accurate statistical models of diffusion coefficients from observations, stressing the use of an average of individual observation-specific diffusion coefficients rather than averaging the inputs before the diffusion coefficients are created, as we have done presently. Watt et al. (2021) further demonstrated that diffusion simulations of electron loss due to plasmaspheric hiss are sensitive to variability time scales, which revealed more diffusion from averaged diffusion coefficients calculated for individual observation-specific diffusion coefficients than when the diffusion coefficients are constructed from averaged inputs. Nevertheless, constructing the diffusion coefficients using averaged inputs is still an important method that numerous studies relied on to reproduce the essential feature of the radiation belt electron dynamics (e.g., Claudepierre et al., 2020; D. Wang & Shprits, 2019; D. Wang et al., 2019; Horne et al., 2013; Hua et al., 2020; H. Zhu et al., 2019; L. T. Li et al., 2017; Q. Zhu et al., 2021). Therefore, understanding the effects of uncertainties in the key inputs of the radiation belt electron simulation is a prerequisite to improve the radiation belt model performance, confidence, and forecasting accuracy.

Ensemble modeling has played an important role in forecasting in various fields including meteorology and oceanography for several decades, but has only been used in the space physics community for about 20 years (Guerra et al., 2020; Schunk et al., 2014). Ensemble modeling is a numerical method that uses a group of predictions with slightly different initial or boundary conditions (e.g., Berner et al., 2011; Cash et al., 2015; Chen et al., 2018; Dumbović et al., 2018; Greybush et al., 2017; Mays et al., 2015; Migliorini et al., 2011; Morley et al., 2018), as done here, or multiple various forecast models (e.g., Abhilash et al., 2018; Kalnay, 2019; Krishnamurti et al., 2000; Schunk et al., 2016; Storer et al., 2019) to generate a broad sample of the possible future states of a dynamic system (Knipp, 2016). Therefore, one of the main strengths of ensemble simulation is that it can help us understand how the uncertainty propagates in the model, as well as the confidence intervals and range of predicted model outcomes, which are important to improve space weather predictions and understand how far a given simulation might be from the true value (Morley, 2020; Murray, 2018). For example, Chen et al. (2018) used the ensembles to assess the impact of uncertainties in electric field boundary conditions on ring current simulations. Camporeale et al. (2016) presented the first ensemble study to quantify how the uncertainties in the input parameters propagate in radiation belt electron simulations by perturbing three key input parameters including the geomagnetic *Kp* index, the maximum latitude extent of chorus waves, and the electron density. However, due to the simple assumption of Gaussian distributions for input sampling and the lack of comparison between ensemble simulations with observations in their study, the impact of inaccuracies of the inputs on the radiation belt electron simulations is still understood in a limit way. Watt et al. (2021) and Thompson et al. (2020) demonstrated using ensembles that the temporal variation of diffusion coefficients in the Fokker-Planck equation is vitally important, the solutions of which depend sensitively on the timescale of the

variation of the diffusion coefficients, as well as the amount of variation in the diffusion coefficients. The study of Hua, Bortnik, Kellerman, et al. (2022) performed event-based ensemble simulations of electron flux decay due to plasmaspheric hiss, where they sampled the distributions of four key input parameters based on Van Allen Probes measurements during a typical event. By comparing the ensembles with observations, the uncertainties in the hiss wave amplitude were shown to dominate the simulation errors compared to total electron density, hiss wave peak frequency, and background magnetic field. Although the authors obtained the distributions based on observations, their event-based sampling is still confined within a limited spatiotemporal coverage of 6 days, which is insufficient to provide good estimations of extreme cases and complete distributions of these four key inputs at a global scale.

In the present study, we perform an ensemble of quasi-linear diffusion simulations of a typical outer radiation belt electron acceleration event at $L = 5.2$ due to whistler-mode chorus waves during the storm of 9 October 2012, which has been comprehensively investigated by Thorne et al. (2013). As chorus waves are believed to be primarily responsible for the observed electron acceleration in this case (Thorne et al., 2013), we similarly limit our study to the two-dimensional diffusion simulation, where only chorus waves are included. Radial diffusion can also contribute to electron acceleration, but this is believed to be a smaller contributor for this event and is thus beyond the scope of the current study. Similar to the study of Hua, Bortnik, Kellerman, et al. (2022), we use percentiles to sample the distributions of inputs and analyze the impacts of the following four key parameters: (a) lower-band chorus wave amplitude (B_w), (b) lower-band chorus wave peak frequency (f_m), (c) background magnetic field (B_0), and (d) total electron density (N_e). There are 11 points used to sample the possible range of each input parameter, leading to 11^4 (∼14,600) ensemble members. Moreover, we sample the distributions based on a superposed epoch analysis of 11 storms that are relatively similar to the storm of 9 October 2012 in terms of simultaneous observations of electron acceleration and chorus wave activities. In this way, the data sampling is improved in terms of better spatiotemporal coverage and better coverage for extreme cases when the inputs are sampled during various storm events comparing to the input sampling based on a single event in the study of Hua, Bortnik, Kellerman, et al. (2022). Based on ensemble simulations, our aim is to quantify the effects of uncertainties in the input parameters on the simulated electron acceleration, which is crucial for uncertainty quantification of the radiation belt electron modeling and for improvement of the radiation belt electron predictions.

The paper is organized as follows. In Section 2, a superposed epoch analysis of 11 similar storms is performed, which enables sampling the distributions of key input parameters based on Van Allen Probes observations and describe the details about the model setup of ensemble simulations. Section 3 presents the comprehensive analysis of our ensemble simulations to examine how the uncertainties in the input parameters influence the electron acceleration and their relative importance to the simulation errors. The conclusions and discussions are presented in Section 4.

2. Data Sampling and Model Description

2.1. Inputs Sampling Based on Van Allen Probes Observations

The Van Allen Probes provide high-quality plasma wave and particle measurements with a perigee at ∼1.1 R_E and an apogee of ∼5.8 R_E (Mauk et al., 2013). The Electric and Magnetic Field Instrument Suite and Integrated Science (EMFISIS; Kletzing et al., 2013) data are used to analyze the chorus wave properties, the background magnetic field, and the total electron density (Kurth et al., 2015). We adopt the differential pitch-angle resolved electron flux data from the Energetic Particle Composition and Thermal Plasma suite (ECT; Spence et al., 2013), with energetic electrons (<1 MeV) measured by Magnetic Electron Ion Spectrometer (Blake et al., 2013; Claudepierre et al., 2021), and relativistic electrons (≥1.8 MeV) measured by Relativistic Electron Proton Telescope (Baker et al., 2013, 2021). The L-shell used in this study is the McIlwain L-shell calculated using TS04D magnetic field model (Tsyganenko & Sitnov, 2005). The OMNIWeb data of geomagnetic indices provide the measurements of SYM-H index with time resolution of 1 min.

We selected 11 storms to perform a superposed epoch analysis, with the detailed $(\text{SYM-H})_{\text{min}}$ and the corresponding time, and the MLT when the satellite was close to the apogee of the selected storms listed in Table S1 in Supporting Information S1. During the selected 11 storms, the coverage of Van Allen Probes in MLT span from night to morning sectors at the L-shell that we focus on, which is favorable for the observations of chorus waves (Meredith et al., 2020). Moreover, the magnitude of the storms as indicated by the $(\text{SYM-H})_{\text{min}}$ in Table S1 in

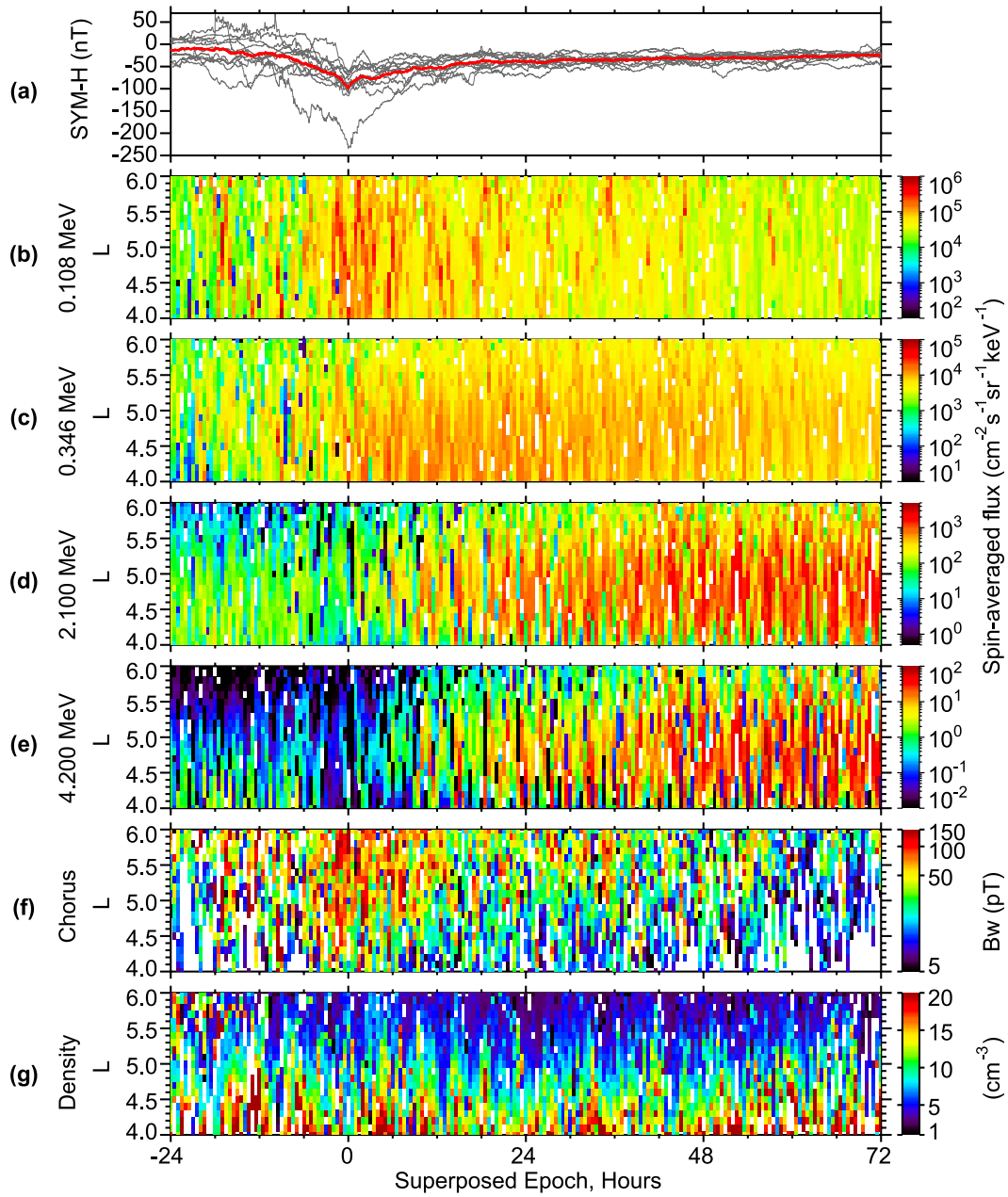

Figure 1. Simultaneous observations of relativistic electron acceleration and chorus wave activities during the selected 11 storms. Superposed epoch analysis results of (a) SYM-H index for the chosen 11 geomagnetic storms (shown as gray lines), with the red line showing the mean profile. Mean values of (b–e) electron spin-averaged fluxes at the indicated energies, (f) lower-band chorus wave amplitude, and (g) electron density as a function of L-shell during the selected 11 storms where both multi-MeV electron acceleration and chorus waves were observed. The spin-averaged electron flux data from Magnetic Electron Ion Spectrometer (Blake et al., 2013) are used in panels (b and c), and Relativistic Electron Proton Telescope (Baker et al., 2013, 2021) data are used in panels (d and e).

Supporting Information S1 varies significantly during different storms. Therefore, the chorus wave activities, the electron density, and the background magnetic field can vary in different storms, which can potentially improve the input sampling in terms of better coverage of extreme cases. The detailed methods of superposed epoch analysis are described in Text S1 in Supporting Information S1.

Figure 1a shows the SYM-H index for the chosen 11 geomagnetic storms (shown as gray lines), with the red line showing the mean profile. Figures 1b–1e present the superposed epoch analysis results of the means of electron

spin-averaged fluxes at energies from 0.1 to 4.2 MeV aligned by the time of $(SYM\text{-}H)_{min}$ in each storm. Significant injections can be frequently observed as shown by the sudden electron flux enhancements at 0.1 MeV. Seed electron fluxes at hundreds of keV were firstly rapidly elevated by about one order of magnitude during the main phase of the storm ($t_{epoch} \sim 0$ hr, where t_{epoch} is the superposed epoch time), and then slowly decreased and remained at a relatively stable level during the recovery phase, which is consistent with the study of Hua, Bortnik, and Ma (2022) indicating that these energetic electrons reached the upper limit of acceleration by chorus. Electron fluxes at multi-MeV started to increase at $t_{epoch} > \sim 12$ hr, with a longer time delay at higher energy, which is consistent with the characteristic feature of the energy-dependent electron acceleration by chorus waves (Horne et al., 2005; Thorne et al., 2013; W. Li, Ma, et al., 2016). Note that the magnitude and rate of the electron acceleration varies in different storms, possibly due to different intensities and durations of chorus waves, and various intensities of radial diffusion. Using the same chorus identification criteria as W. Li, Santolik, et al. (2016), Figure 1f shows the wave amplitude of lower-band chorus waves. The intense chorus waves were mostly observed associated with injections as indicated in Figure 1b, especially during the main phase of the storm with the most significant injections. During the electron acceleration process, the observed electron densities were mostly smaller than 10 cm^{-3} at $L > \sim 5$, which is lower than the empirical density model of the plasma trough from Sheeley et al. (2001). For example, the observed density is around ~ 5 cm^{-3} at $L = 5.5$, which is smaller than 11 cm^{-3} from Sheeley et al. (2001) without considering the MLT factor. This observed lower electron density is favorable for the local electron acceleration at multi-MeV by chorus waves (Allison et al., 2021; Thorne et al., 2013).

As our ensemble modeling is based on a typical event during the storm of 9 October 2012, we sample the distributions of the normalized four input parameters at $L = 5.2$ based on superposed epoch analysis using Van Allen Probe measurements during the selected 11 storms, which are shown in Figures 2a–2d. Here, the inputs are normalized by the median value in each storm, and the inputs sampling time period is selected when the chorus wave amplitude was intense (shown in Figure 1f) so that chorus waves can potentially contribute significantly to electron acceleration. In addition, this time period is close to the simulation time period, which will be described below. Due to the reason that the ensemble simulations will be compared to the event-specific electron flux observations during the storm of 9 October 2012, we analyze the relative variation of the inputs using normalized results with respect to the median values in each storms instead of the absolute values, which results in an overall distribution of values that is realistic and makes sense. Among these four input parameters, the variation of the background magnetic field (B_0) is the smallest, which deviates from the median value by less than a factor of 0.5. In contrast, the uncertainties in the observed electron density (N_e), the wave peak frequency (f_m/f_{ce}), and the wave amplitude (B_w) of lower-band chorus waves are much more significant, which will potentially cause larger simulation errors compared to B_0. We note that the normalized distributions of input can be sensitive to the selected sampling time period. But outside the current selected time period, the wave intensity of chorus drops quickly, leading to larger relative variation with respect to the median value in each storm.

The histograms of the normalized sampled inputs are shown in Figures 2e–2h, with the blue star lines representing the sampled normalized input parameter distributions using percentiles. Similar to Hua, Bortnik, Kellerman, et al. (2022), we choose 11 levels for each input, corresponding to the percentiles of 1%, 5%, 16%, 25%, 36%, 50%, 62%, 74%, 84%, 95%, and 99%, leading to 11^4 (14,641) members in our ensemble. The sampled distributions of the normalized inputs are then multiplied by the median value observed during the 9 October 2012 storm to calculate the absolute value of the ensemble simulation inputs, which does not vary with time so that we can separate the impact of individual input parameters. In this way, the inputs with the 50th percentile in the ensembles is the same as the event-based median values during the case that we focus on. The observed evolutions of these four inputs during the 9 October 2012 storm are shown in Figure S1 in Supporting Information S1, whose median results are: B_w(median) = 69.91 pT, f_m/f_{ce}(median) = 0.23, B_0(median) = 221.14 nT, and N_e(median) = 3.80 cm^{-3}. We adopt the statistical distribution of wave amplitudes in different MLT sectors (Meredith et al., 2020) and scale it based on the sampled values to calculate the drift- and bounce-averaged diffusion coefficients. The root mean square of the B_w in different MLT sectors is the same as the sampled absolute value. We assume that the lower-band chorus waves have a Gaussian frequency spectrum distribution (Glauert & Horne, 2005), with $\delta f/f_{ce} = 0.08$, $f_{lc}/f_{ce} = 0.05$, and $f_{uc}/f_{ce} = 0.5$ (W. Li, Santolik, et al., 2016). Here, δf is the bandwidth rolloff scale, and f_{lc} and f_{uc} are the lower and upper frequency limits. We use a frequently adopted quasi-parallel Gaussian wave normal angle distribution with $\theta_m = 0°$, $\theta_w = 30°$, $\theta_{lc} = 0°$, and $\theta_{uc} = 45°$ (e.g., Hua, Bortnik, & Ma, 2022; Hua et al., 2018; Thorne et al., 2013), where θ_m is the wave angle with peak power, θ_w

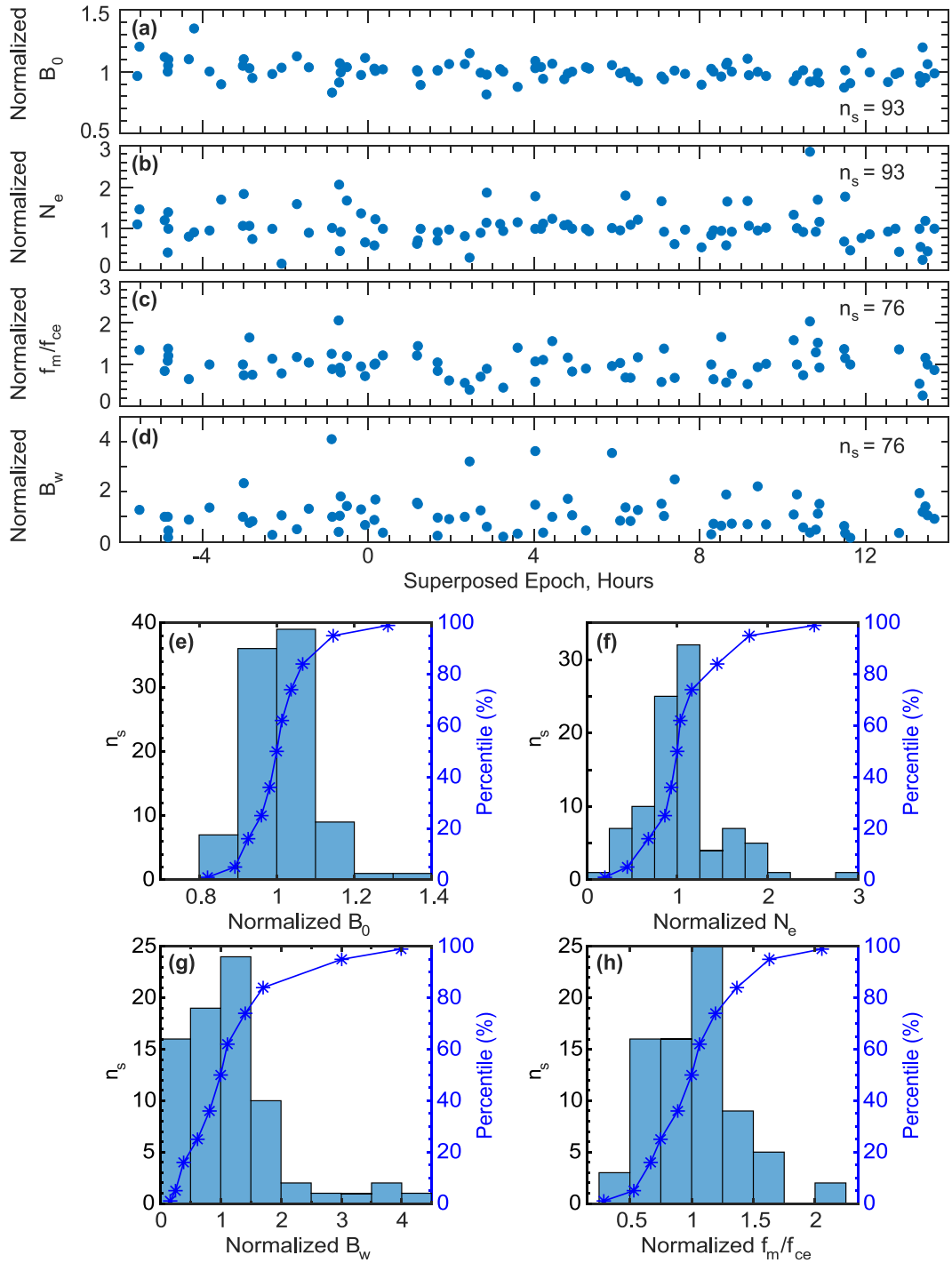

Figure 2. Sampling distributions of normalized input parameters at $L = 5.2$ based on superposed epoch analysis using Van Allen Probe measurements during the selected 11 storms. The sampling points are recorded every time when satellite crossed $L = 5.2$ without binning in time. Superposed epoch analysis of normalized results of (a) background magnetic field projected to the geomagnetic equator (B_0), (b) total electron density (N_e), (c) lower-band chorus peak wave frequency (f_m) normalized by the electron gyrofrequency at equator (f_{ce}), and (d) lower-band chorus wave amplitude (B_w). Here, the results are normalized by the median results during each storm. The total sample number (n_s) are marked for each input. Histogram of the normalized (e) background magnetic field, (f) electron density, (g) wave amplitude, and (h) normalized wave peak frequency of lower-band chorus waves by f_{ce}, with the blue star lines representing the sampled normalized input parameter distributions using percentiles.

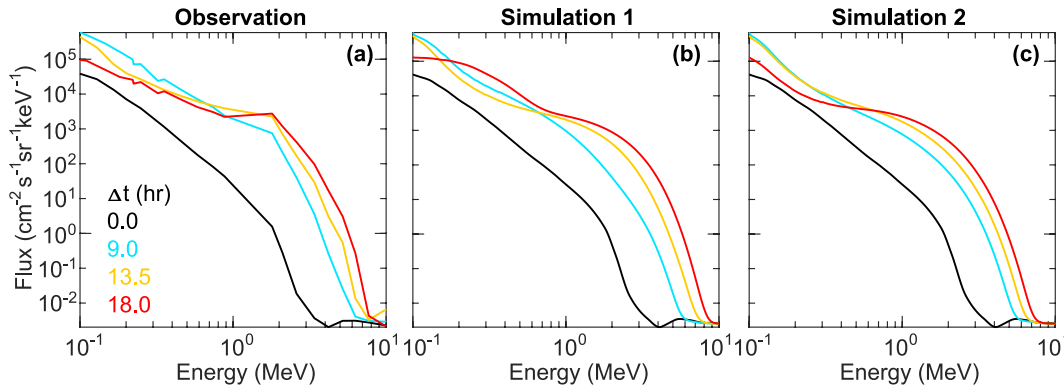

Figure 3. The comparison of the temporal evolution of omnidirectional electron fluxes during the 9 October 2012 storm as a function of energy at color-coded times from 0 till 18 hr at $L = 5.2$ from (a) observation, (b) simulation where time-varying input parameters based on observations are adopted, and (c) simulation where the 50th percentiles of all input parameters are adopted. Results in the next figures will be extracted at these four times.

the angular width, and θ_{lc} and θ_{uc} the lower and upper limits. The latitudinal coverage of chorus waves varies in different MLT sectors and is based on the statistical results from Meredith et al. (2012).

2.2. Radiation Belt Model Description

We use the geomagnetic storm event on 9 October 2012, with the assumption that chorus waves dominate the electron acceleration, for the ensemble analysis. The method to obtain event-specific diffusion coefficients using pre-computed diffusion matrix was developed in 2019 and applied to the rapid prediction of radiation belt dynamics in the presentation of Bortnik et al. (2019). The detailed methodology was described in Supporting Information of Hua, Bortnik, Kellerman, et al. (2022), and named as "Look-up Table" method thereafter. We employ this method to rapidly estimate the bounce-averaged quasi-linear diffusion coefficients. By numerically solving the two-dimensional Fokker-Planck diffusion equation (e.g., Xiao et al., 2009), we perform the simulations at the energy range of 0.1–10 MeV at $L = 5.2$ over a period of 18 hr, which is the region where the growing peak of the electron PSD was observed. The electron PSD (f) is related to the differential flux (j) as $f = j/p^2$, where p is the electron momentum. The initial electron PSD distribution is collected at ~18:30 UT on 8 October 2012 when Van Allen Probe B crossed $L = 5.2$. The pitch-angle resolved electron flux data may not provide full coverage of electron fluxes from 0° to 90° equatorial pitch angle, so we assume the initial pitch angle distribution takes the simple analytical form $f(\alpha_{eq}, p) = f(\alpha_{eq} = 90°, p)\sin\alpha_{eq}$, which has been widely used in the previous studies (e.g., Hua et al., 2018; Thorne et al., 2013). We adopt a time-varying lower energy boundary based on Van Allen Probes measurements to include the injections at 0.1 MeV energy, and the electron PSDs at the upper energy boundary are set as constants. We take $f = 0$ inside the bounce loss cone, and $D_{\alpha\alpha}\frac{\partial f}{\partial \alpha} + D_{\alpha p}\frac{\partial f}{\partial p} = 0$ at $\alpha_{eq} = 90°$ following previous studies (Albert et al., 2016; Hua, Bortnik, Kellerman, et al., 2022).

3. Ensemble Simulations

3.1. Simulation Baseline

Figure 3 displays the comparison of temporal evolutions of normalized omnidirectional electron fluxes during the 9 October 2012 storm as a function of energy at color-coded times at $L = 5.2$ from observation (Figure 3a) and simulation (Figure 3b) where time-varying input parameters based on observations are adopted (labeled as simulation 1). Note that the observed electron fluxes were not always available over the full equatorial pitch angle range from 0° to 90°. Therefore, in the present study, we calculate the normalized omnidirectional flux of $J = \frac{\int_{\alpha 1}^{\alpha 2} j(\alpha)\sin\alpha d\alpha}{\int_{\alpha 1}^{\alpha 2}\sin\alpha d\alpha}$, where all the available measurements at different pitch angles are included. The simulated relativistic electron fluxes reproduced identically to Thorne et al. (2013) with an event-driven computation based on using the local measured properties, which remarkably agree with the observation, with the most significant acceleration at energies between ~2 and 5 MeV, further confirming the dominant role of local wave acceleration

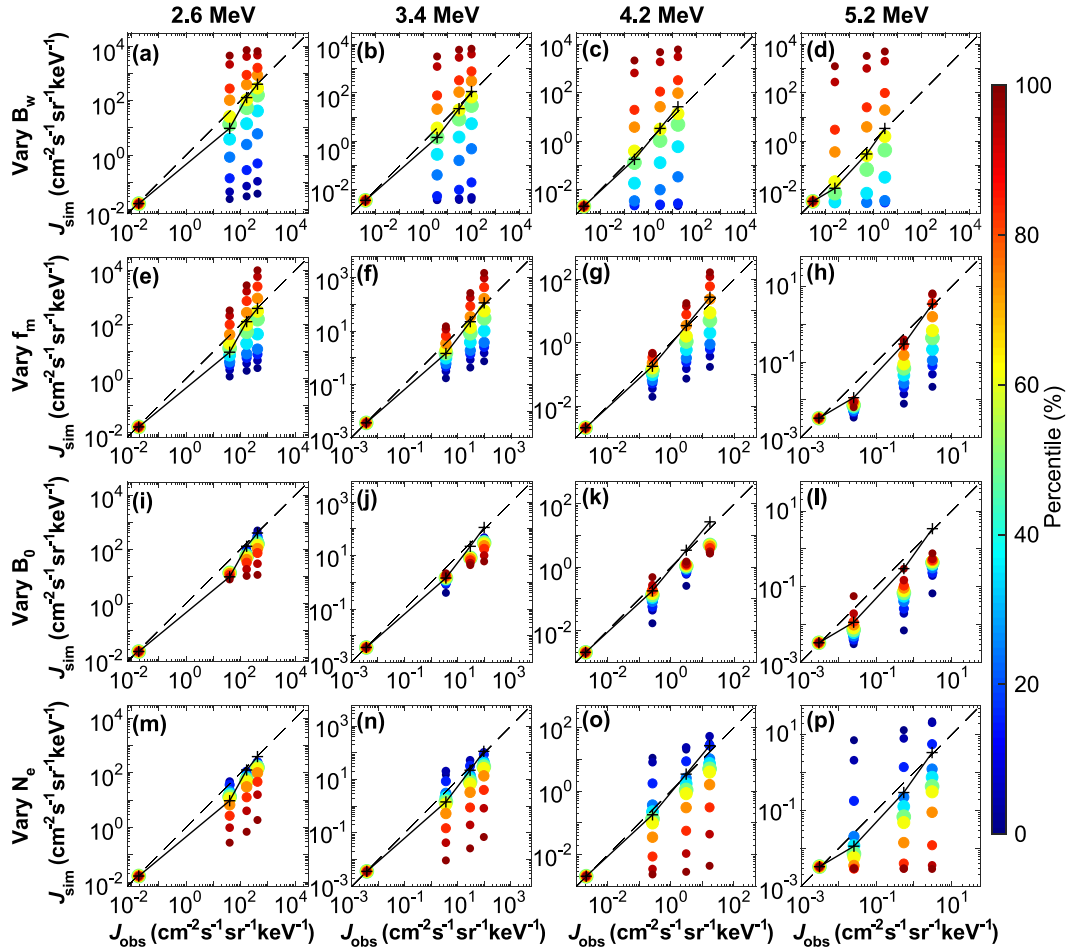

Figure 4. Regression analysis of the ensemble simulations obtained by only varying one input parameter at a time, while the 50th percentiles of the other three inputs are adopted, showing the simulated electron fluxes (J_{sim}) versus observed fluxes (J_{obs}) color-coded by the percentile of input parameters of (a–d) chorus wave amplitude, (e–h) chorus wave peak frequency, (i–l) background magnetic field, and (m–p) electron density at indicated four energies. The solid lines connecting the plus symbols correspond to the simulated results where time-varying input parameters based on observations are adopted. Each column of symbols represents the simulation time of 0, 9, 13.5, and 18 hr. The dot size changes and increases with error decreasing.

by chorus (Thorne et al., 2013). The electron acceleration in the simulation where the 50th percentiles of all input parameters are adopted (the inputs does not vary with time, and labeled as simulation 2, shown in Figure 3c) is slightly slower than simulation 1 using the local measurements, possibly due to slightly smaller chorus wave amplitude. However, simulation 2 is still consistent with the essential feature of the observed electron acceleration at multi-MeV. For the sake of simplicity, we consider simulation 2 as the baseline in our ensemble simulations for the following uncertainty quantification and the inputs for the ensemble simulations does not vary with time so that we can separate the effects of perturbations in each input on the simulation results.

3.2. Uncertainty Quantification

3.2.1. Varying Only One Input Parameter

Figure 4 presents the regression analysis of the ensemble simulations where we vary only one input parameter at a time, while the other three inputs are kept fixed using 50th percentiles. Each panel shows the simulated omnidirectional electron fluxes (J_{sim}) versus observed fluxes (J_{obs}) color-coded by the percentile of input parameters of (a–d) chorus wave amplitude, (e–h) chorus wave peak frequency, (i–l) background magnetic field, and (m–p) electron density at the indicated four energies. The lines connecting the "plus" symbols correspond to

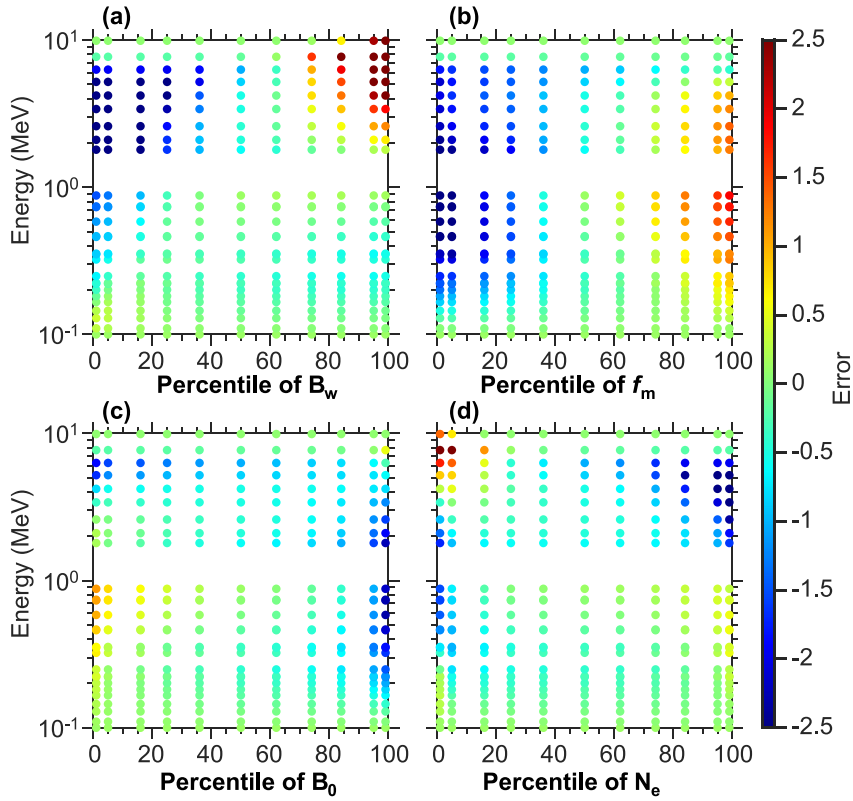

Figure 5. The error of log accuracy ratio of the electron flux at the end of the simulation time period (18 hr) as a function of energy and percentile of (a) chorus wave amplitude, (b) chorus wave peak frequency, (c) background magnetic field, and (d) electron density by only varying one input on the horizontal axis while the 50th percentiles of other three inputs are adopted.

the simulated results where time-varying input parameters based on observations are adopted. Here, the size of each colored dot is proportional to (100% − |a% − 50%|), where a% corresponds to the varying percentile of the inputs. In order to emphasis the lowest error, the results of the simulation baseline with 50th percentile of all four inputs are shown as the green dots with largest size. The comparison is evaluated at 4 time snapshots corresponding to those shown in Figure 3, and displayed in such a way that the dots from left to right corresponding to the initial fluxes and the fluxes at the end of the simulation (18 hr) in each panel. Similar as the study of Hua, Bortnik, Kellerman, et al. (2022), the perturbations in chorus wave amplitude B_w cause the largest deviation of the simulated electron acceleration from observations compared to the other three input parameters, with a stronger value of B_w leading to a more intense response of relativistic electrons to chorus acceleration (dark red dots in Figures 4a–4d). Unlike the results from the study of Hua, Bortnik, Kellerman, et al. (2022) where the uncertainties in the other three inputs have relatively minor impacts on the simulation results, the inaccuracy in chorus wave peak frequency f_m, background magnetic field B_0, and electron density N_e also cause significant deviation in the simulation. While larger f_m and smaller N_e are more favorable for multi-MeV electron acceleration, the influence of N_e is slightly more significant than f_m for electrons above 3 MeV. In addition, since the geomagnetic field can become stretched and hence less dipolar during the storm time (Tsyganenko et al., 2003), the changing B_0 also play an important role in affecting the simulated electron acceleration by chorus, which causes an opposite trend for different energies due to its impact on the ratio of f_{pe}/f_{ce}. (where f_{pe} and f_{ce} represent the electron plasma frequency and gyrofrequency, respectively).

To quantify the simulation errors, Figure 5 shows the simulation errors calculated by using the log accuracy ratio of $\log_{10}(J_{sim}/J_{obs})$ (Morley et al., 2016) obtained at the end of the simulations at 18 hr. The log accuracy ratio is symmetric for over- and under-estimation, with the error of 1 (−1) representing that the simulation (observation) is 10 times higher than the observation (simulation). The largest simulation errors are associated with the most intense B_w, suggesting the dominant role of uncertainties in B_w in causing simulation errors, which is somewhat different from the results obtained by Camporeale et al. (2016) who found that the uncertainties in density have

the dominant impact on simulated electron acceleration by chorus. Nevertheless, consistent with Camporeale et al. (2016), our results demonstrate that the second largest simulation errors for multi-MeV electron acceleration are associated with the lowest electron density. These errors are larger than the simulation errors when varying f_m. The changing B_0 overall leads to the smallest deviation of simulations from observation. Therefore, the impact of the inaccuracy of the input parameters on the simulation performance follows the order of error magnitude: Err(B_w) > Err(N_e) > Err(f_m) > Err(B_0).

3.2.2. The Effect of Varying Two Input Parameters

Figure 6 presents the simulation errors obtained by varying the two inputs indicated on both the vertical axis (percentile of chorus wave amplitude) and horizontal axis (from left to right: percentile of background magnetic field, chorus wave peak frequency, and electron density), while 50th percentile is adopted for the left two input parameters. The color-coded curves represent the contour of the isolines. Overall, the perturbations in all the four input parameters can significantly influence the simulation. The largest simulation errors for both overestimation (shown as the red color) and underestimation of acceleration (shown as the blue color) are always associated with the extreme cases of B_w, while smaller B_0 and N_e, and larger f_m are more favorable for multi-MeV electron acceleration by chorus scattering, and vice versa.

3.2.3. The Worst Cases in the Ensemble Simulations

To estimate the worst-case performance of the diffusion simulations obtained when there are uncertainties in the key input parameters, we identify the largest and smallest simulation errors (i.e., the simulated strongest and weakest electron acceleration) for each energy and their corresponding percentiles of input parameters, which are shown in Figure 7. The simulation errors of strongest acceleration increase with energy, reaching ∼8 orders of magnitude larger than the observations at ∼7 MeV (Figure 7a). The simulations showing strongest acceleration are mostly caused by combinations of inputs having the largest B_w and f_m, together with the smallest N_e and B_0. In contrast, the case for the combination of distributions of input parameters associated with the weakest acceleration is more complicated (Figure 7b). The simulation errors decrease with decreasing energy. Due to the shift of resonance energy when changing f_m, N_e, and B_0, electron fluxes below 3 MeV are reduced instead of being elevated with smallest f_m, 16th percentile of N_e, and largest B_0. Therefore, the strongest value of B_w leads to the most significant underestimation of acceleration in the simulation. However, there is no electron flux decay above 3 MeV in our ensemble no matter how inputs vary. Therefore, multi-MeV electron fluxes barely change in the simulations with largest N_e and smallest f_m, resulting in the smallest simulation errors (weakest acceleration), that is, the difference between the initial condition and the multi-MeV flux observation remains similar during the 18 hr of the simulation. It is straightforward to understand that a weaker B_w will lead to a weaker acceleration up to no change. However, the weakest acceleration for electrons above ∼5 MeV is mainly determined by the largest N_e and is not sensitive to B_w and B_0. A caveat of this approach is that extreme value of one (or more) parameters can hide the weaker role of others, as we seem to see with f_m that is not responding for the case of the weakest acceleration and peaking up at 1%. Here, that is further accentuated because on top of that B_w is weak.

3.2.4. Probabilistic Approach

Following the study of Hua, Bortnik, Kellerman, et al. (2022), we employ a similar method to turn this physics-based deterministic model into a probabilistic problem. We first use Gaussian fitting $\frac{1}{\sigma\sqrt{2\pi}}\exp\left(-0.5\times\left(\frac{x-\mu}{\sigma}\right)^2\right)$ to get the individual probability density function (PDF) of the four normalized input parameters as shown in Figure 2, shown as the red lines in Figures 8a–8d with the mean value (μ) and standard deviation (σ) given at the top right corner in Figures 8a–8d. Here, x is the value of each of the normalized input parameters, which is unitless. Therefore, the PDF here is also unitless. The integration of individual PDF for each input parameters is 1. Based on these fitting results, the probability density for each point of the sampled inputs is shown as the red dots in the same panels. For simplicity, we assume that the four input parameters are independent, so that the combined probability density of an ensemble member is the product of the probability densities attributed to the four inputs corresponding to this member. For instance, the probability density for an ensemble member with inputs of B_{w0}, f_{m0}, N_{e0}, and B_{00} equals PDF(B_{w0}) × PDF(f_{m0}) × PDF(N_{e0}) × PDF(B_{00}). This approximation seems reasonable since the 1D posterior density and 2D marginal distributions of the four input parameters based on Bayesian inference (e.g., Sarma et al., 2020) shown in Figure S2 in Supporting Information S1 suggest that there is not a clear correlation among these four inputs. The detailed analysis based on Bayesian framework is described in Text S2 in Supporting Information S1. Since the distributions of the PDF of the normalized inputs are based on the direct

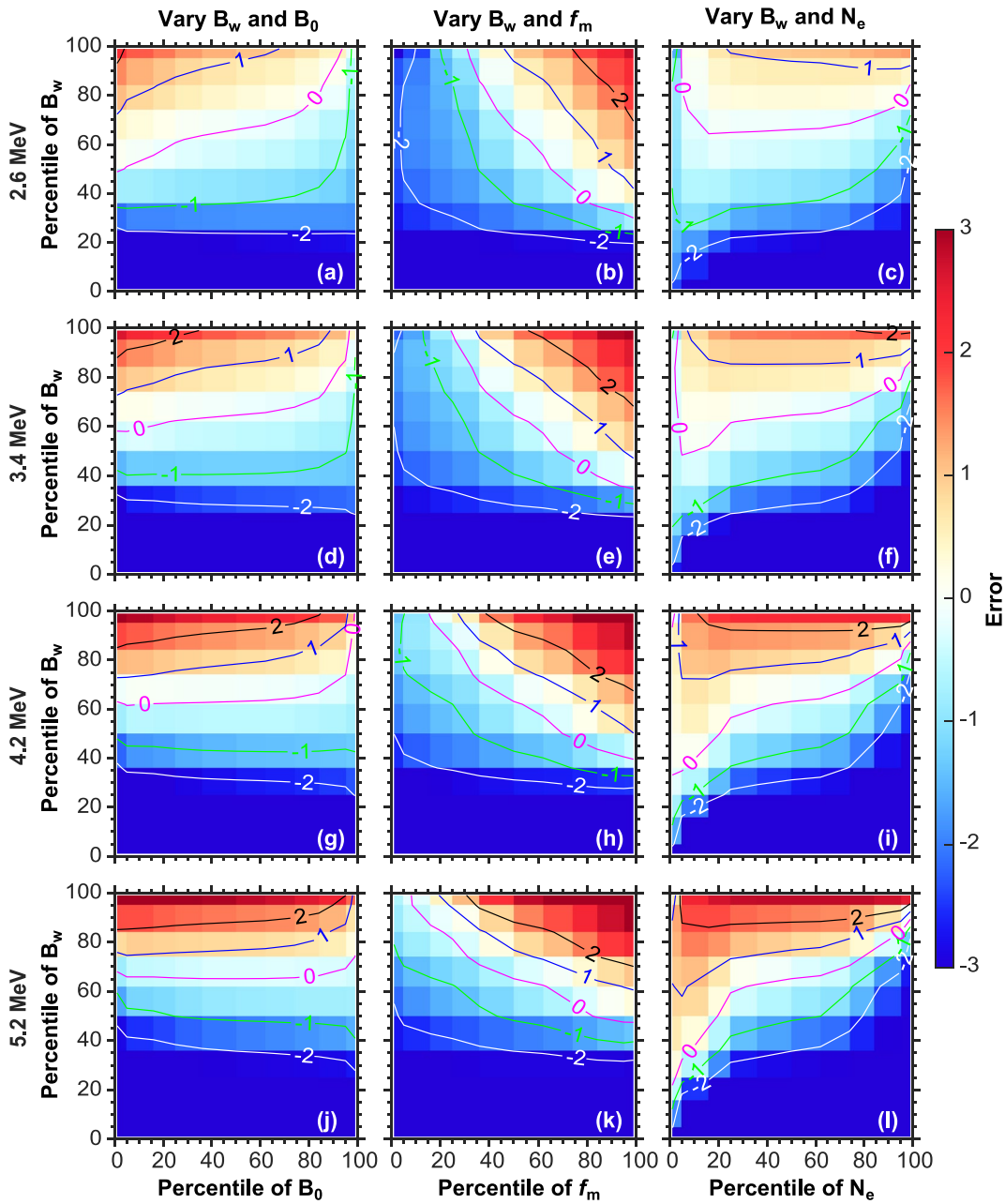

Figure 6. The error of log accuracy ratio at the end of simulations (18 hr) obtained by only varying the two inputs on the vertical axis (percentile of chorus wave amplitude) and horizontal axis (from left to right: (a, d, g, and j) percentile of background magnetic field, (b, e, h, and k) chorus wave peak frequency, and (c, f, i, and l) electron density), while 50th percentile is adopted for the left two input parameters. The color-coded curves represent the contour of the isolines.

in situ observations during multiple storms, the probability density calculated here can help us understand the probability of the possible combinations of the four inputs in the real magnetosphere.

The distribution of probability density versus the simulation error of each ensemble member is shown in Figures 8e–8h as dots, where the red and blue colors show the overestimation and underestimation of electron acceleration, respectively. These results are further binned into a probability density grid that is uniformly distributed in logarithmic space from 10^{-11} to 10 with 21 points in total. The median simulation errors of the overestimation and underestimation of electron acceleration are shown as the red and blue circles with upper and lower quartiles as error bars. Overall, the magnitude of the simulation error with error >0 decreases with increasing

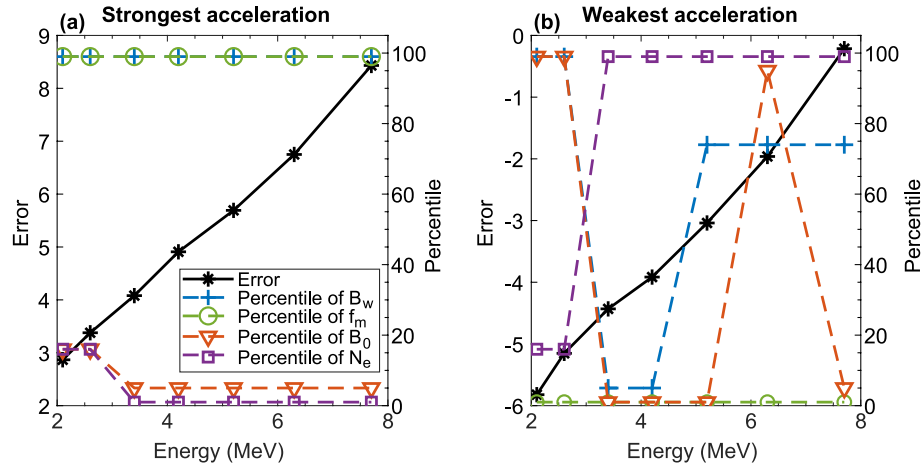

Figure 7. The error of log accuracy ratio (black star lines) of the strongest (a) and weakest (b) electron acceleration in the ensemble simulations as a function of electron energy, with corresponding percentiles of chorus wave amplitude (blue lines plus symbols), chorus wave peak frequency (green lines circle symbols), background magnetic field (orange lines triangle symbols), and electron density (purple lines square symbols). The blue and green lines overlap in panel (a).

probability density for relativistic electrons, with the largest simulation error reaching ∼4 orders of magnitude for electrons above 2.6 MeV, demonstrating that the simulated acceleration can significantly deviate from observations. On the contrary, the simulation errors of the underestimation of acceleration mostly concentrate at the lowest value for the higher energies. The reason is that acceleration at higher energies requires a longer time than the electrons at lower energies. Therefore, electron fluxes at higher energies barely vary if the preferable input parameters are not present, whose simulation error is the difference between the initial condition and the observations. Figure 9 is similar to Figures 8e–8h though it only includes ensemble members with inputs between 36th to 62nd percentiles (±1 standard deviation). The simulation errors are concentrated between ∼−2.0 and 0.5, suggesting that the simulation members with largest probability density still provide a reasonable estimates of radiation belt electron dynamics within a small uncertainty range, which is important for accurate forecast of radiation belt electrons.

4. Discussions

In this section, we discuss the limitations and possible improvements of the present study. Although the input sampling in our study is limited to the selected 11 storms, which cannot provide a comprehensive analysis of the possible variation of the four input parameters, out study has indeed significantly improved it in terms of better spatiotemporal coverage and better coverage for extreme cases comparing to the previous studies (Camporeale et al., 2016; Hua, Bortnik, Kellerman, et al., 2022). We note that our probability results are based on the assumption that the four input parameters are independent for the sake of simplicity, but there can be correlations among these inputs in reality. For example, the study of Allison et al. (2021) demonstrated that electron acceleration reaching >7 MeV only occurs when the electron density is very low, which is mostly associated with strong storms. The geomagnetic field line can be highly non-dipolar and the plasmasphere can be eroded during storm time, potentially causing correlated large variation in both B_0 and N_e. Therefore, future studies are needed to investigate the joint probabilities among these key input parameters (which could in general be complex and nonlinearly dependent on storm phase and intensity) to refine the calculation of probability density. In addition, our study is limited to the diffusive scattering effects in the quasi-linear regime, while the nonlinear effects due to chorus waves could be important (Mourenas et al., 2018, 2022; Zhang et al., 2018). Furthermore, the simulated electron acceleration is not only sensitive to the perturbations in the four key input parameters analyzed in the present study, but also strongly depends on the initial flux distribution and lower energy boundary condition, which have been comprehensively analyzed in previous studies (Allison et al., 2019; Hua, Bortnik, & Ma, 2022; Varotsou et al., 2008) and are beyond the scope of the current study. It is worth noting that the method that calculates the individual observation-specific diffusion coefficients using simultaneous observations of plasma and wave parameters (Ross et al., 2020; Watt et al., 2019, 2021) can be

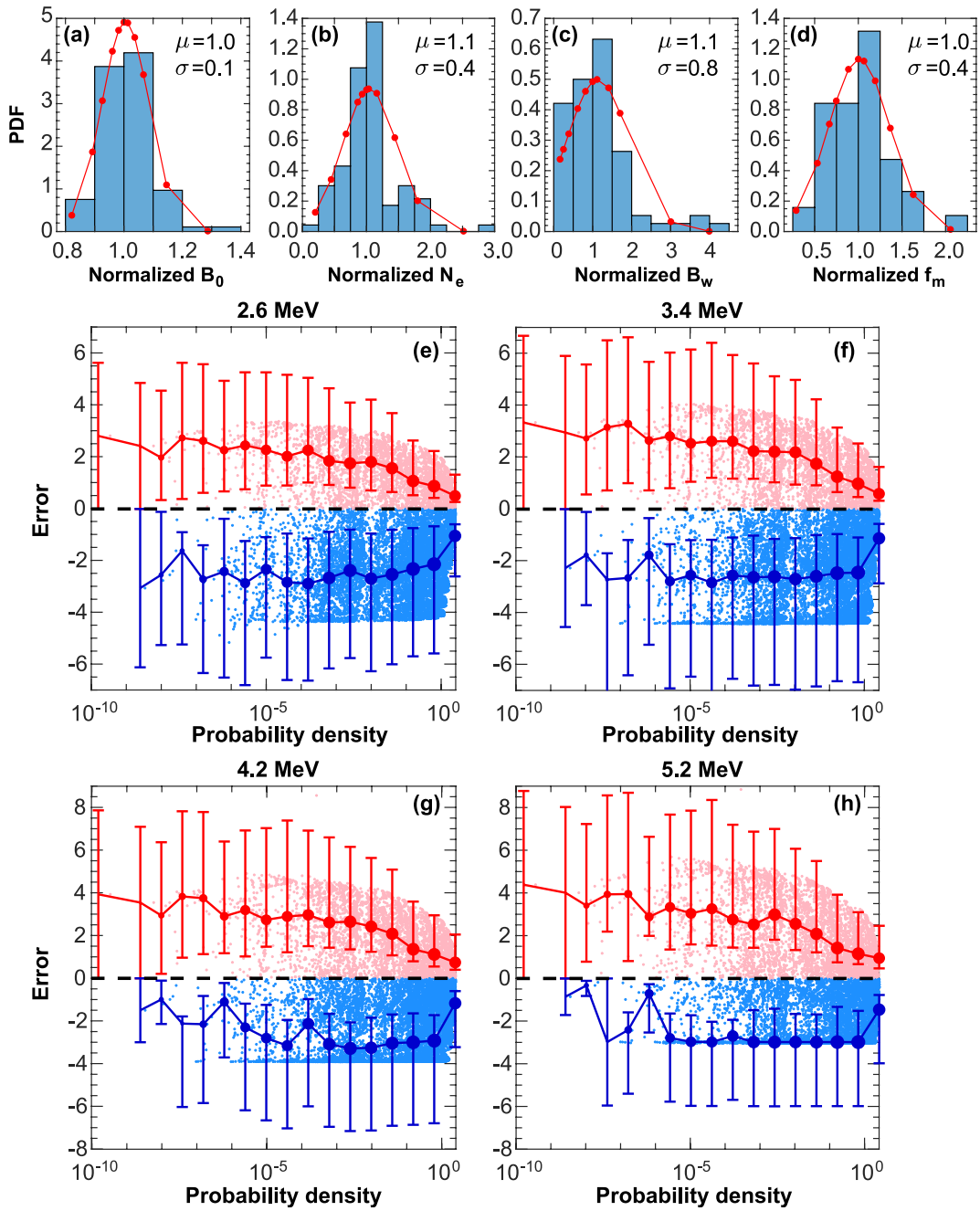

Figure 8. The probability density function (PDF) of the normalized (a) background magnetic field, (b) total electron density, (c) chorus wave amplitude, and (d) chorus wave peak frequency based on superposed epoch analysis using Van Allen Probe measurements during the selected 11 storms. The red lines show the Gaussian fitting of the PDF with the corresponding mean value (μ) and standard deviation (σ) given at the top right corner in each panel. (e–h) The simulation error (i.e., log accuracy ratio) of the ensemble simulations versus probability density at indicated energies, with the light red and light blue dots showing the overestimation and underestimation of electron acceleration, respectively. The red and blue dotted lines show the median values, with error bars below and above the dots representing the lower and upper quartiles, respectively.

used to sample the distributions of diffusion coefficients to improve the ensemble simulations in the current study, which will be left to the future study. However, in the present study, we have approached this problem from a perspective that is perhaps closer to real-life space weather prediction, where the uncertainty is given over the range of inputs, and the requirement is to provide the statistical uncertainty of the resulting output fluxes.

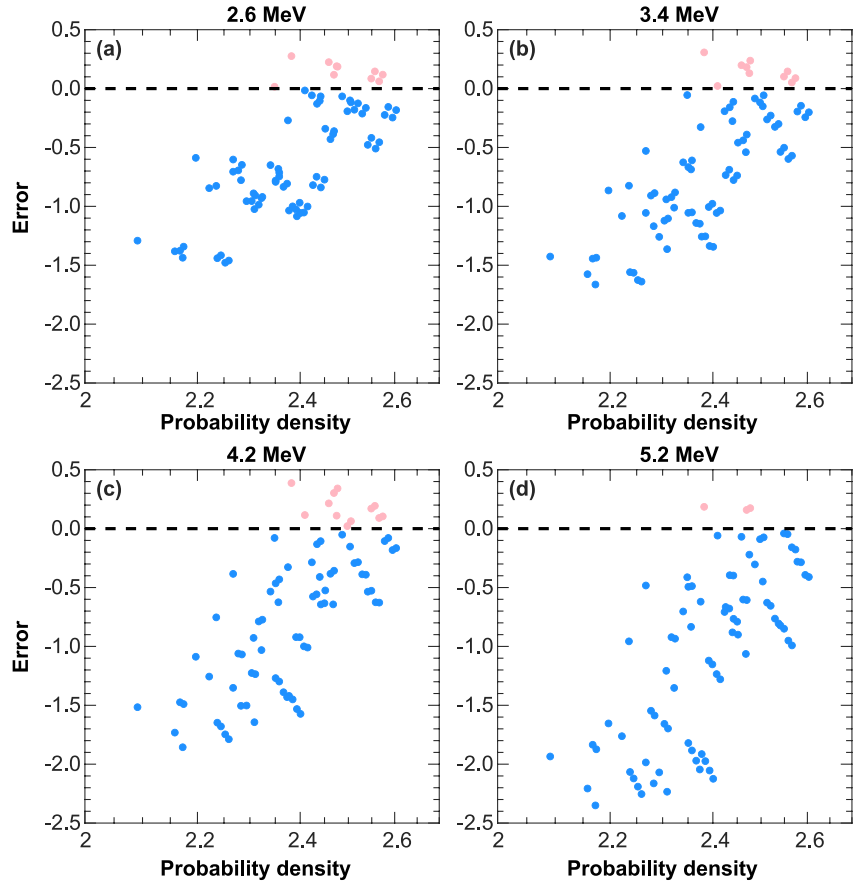

Figure 9. Same as Figures 8e–8h except that only the results of ensemble members with inputs between 36th to 62nd percentiles are plotted. Simulations produce a ∼2 orders of magnitude error comparing to the observations with the inputs between 36th and 62nd percentiles.

5. Conclusions

In the present study, we quantify the influence of uncertainties in the four key input parameters on the wave-induced radiation belt electron acceleration by performing ensemble quasi-linear diffusion simulations during the representative storm on 9 October 2012, where chorus waves dominate electron acceleration at $L = 5.2$. Based on superposed epoch analysis of 11 storms when both multi-MeV electron flux enhancements and chorus wave activities were observed by Van Allen Probes, we use nonparametric statistics (percentiles) to sample the normalized input distributions for the four key inputs to estimate their relative perturbations with respect to the median value in each storm, including chorus wave amplitude B_w, chorus wave peak frequency f_m, background magnetic field B_0, and electron density N_e.

We ran a ∼14,600-member ensemble simulation to systematically analyze the performance of the radiation belt electron model by comparing with the observed electron flux evolution from Van Allen Probes at different energies. Our results demonstrate that the uncertainties in all the four key input parameters can cause significant deviation of the simulated electron acceleration away from the observation, but the dependence varies with both electron energy and whether acceleration overestimation or underestimation is considered. Larger chorus wave amplitudes and peak frequencies, and lower electron densities are more favorable for multi-MeV electron acceleration. Although the variation in B_0 plays a less important role in causing simulation error, its influence is still nonnegligible compared with its impact on electron loss driven by plasmaspheric hiss at lower L-shell (Hua, Bortnik, Kellerman, et al., 2022). Note that the nondipolar field is not considered in the current study, which can directly change the diffusion coefficients (Ma et al., 2012; Ni et al., 2012; Orlova et al., 2012) and the shape of electron PSD peak (Green & Kivelson, 2004; Loridan et al., 2019). Our results demonstrate the dominant role of the changing B_w in causing simulation errors. Consistent with Camporeale et al. (2016), our results also confirm

that perturbations in electron density can cause significant discrepancy between simulated chorus-driven acceleration and observation. The impact of the uncertainties in the inputs on the simulation accuracy falls into the following sequence of errors: Err(B_w) > Err(N_e) > Err(f_m) > Err(B_0).

By calculating the probability density of the simulation error in our ensemble, we turn this physics-based deterministic radiation belt model into a probabilistic one, which gives the prediction of electron dynamics along with the confidence of simulation performance. Overall, the magnitude of the simulation error with errors >0 decreases with increasing probability density for relativistic electrons, while the simulation errors of the underestimation of acceleration mostly concentrate at the lowest value for higher energies, due to the fact that higher energy electrons are more difficult to be accelerated without preferable input parameters. In addition, the simulation only deviated from observation within ∼2 orders of magnitude with largest probability density, while the simulations significantly deviate away from observations once the perturbations in the inputs becomes larger, which is important for forecast of radiation belt electrons.

Our study reveals the influence of uncertainties in the key input parameters on the simulated radiation belt electron acceleration by chorus (within the limitations stated above), with the input uncertainties obtained from superposed epoch analysis from multiple similar storms. This type of ensemble-based uncertainty quantification is of paramount importance in understanding the range of errors inherent in radiation belt modeling, the probability of obtaining such errors, for specifying confidence intervals of any given simulation, and for the verification of radiation belt electron models and improvements of accurate electron predictions.

Data Availability Statement

The ECT data were obtained from https://rbsp-ect.newmexicoconsortium.org/data_pub/. The VanAllen probes data from the EMFISIS instrument were obtained from http://emfisis.physics.uiowa.edu/Flight. The geomagnetic indices were obtained from the OMNI data set (https://omniweb.gsfc.nasa.gov/ow_min.html). The source data used to produce figures in the present study are publicly available at https://doi.org/10.6084/m9.figshare.20321670.v1 (Hua et al., 2023).

Acknowledgments
The authors acknowledge the Van Allen Probes mission, particularly the EMFISIS and ECT team for providing the wave and particle data. JB and MH gratefully acknowledge support from subgrant 1559841 to the University of California, Los Angeles, from the University of Colorado Boulder under NASA Prime Grant Agreement 80NSSC20K1580, and NASA/SWO2R Grant 80NSSC19K0239. QM would like to acknowledge the NASA Grant 80NSSC20K0196. ACK would like to acknowledge support from the NASA Grants 80NSSC20K1402 and 80NSSC20K1281, and the NSF Award 2149782. EC is partially supported by the NASA Grants 80NSSC20K1580, 80NSSC20K1275, and 80NSSC21K1555.

References

Abel, B., & Thorne, R. M. (1998). Electron scattering loss in Earth's inner magnetosphere: 2. Sensitivity to model parameters. *Journal of Geophysical Research*, *103*(A2), 2397–2407. https://doi.org/10.1029/97JA02920

Abhilash, S., Mandal, R., Dey, A., Phani, R., Joseph, S., Chattopadhyay, R., et al. (2018). Role of enhanced synoptic activity and its interaction with intra-seasonal oscillations on the lower extended range prediction skill during 2015 monsoon season. *Climate Dynamics*, *51*(9–10), 3435–3446. https://doi.org/10.1007/s00382-018-4089-3

Agapitov, O., Mourenas, D., Artemyev, A., Hospodarsky, G., & Bonnell, J. W. (2019). Time scales for electron quasi-linear diffusion by lower-band chorus waves: The effects of ωpe/Ωce dependence on geomagnetic activity. *Geophysical Research Letters*, *46*(12), 6178–6187. https://doi.org/10.1029/2019GL083446

Albert, J. M., Artemyev, A. V., Li, W., Gan, L., & Ma, Q. (2021). Models of resonant wave-particle interactions. *Journal of Geophysical Research: Space Physics*, *126*(6), e2021JA029216. https://doi.org/10.1029/2021JA029216

Albert, J. M., Starks, M. J., Horne, R. B., Meredith, N. P., & Glauert, S. A. (2016). Quasi-linear simulations of inner radiation belt electron pitch angle and energy distributions. *Geophysical Research Letters*, *43*(6), 2381–2388. https://doi.org/10.1002/2016GL067938

Albert, J. M., Starks, M. J., Selesnick, R. S., Ling, A. G., O'Malley, S., & Quinn, R. A. (2020). VLF transmitters and lightning-generated whistlers: 2. Diffusion of radiation belt electrons. *Journal of Geophysical Research: Space Physics*, *125*(3), e2019JA027030. https://doi.org/10.1029/2019JA027030

Allison, H. J., Horne, R. B., Glauert, S. A., & Del Zanna, G. (2019). On the importance of gradients in the low-energy electron phase space density for relativistic electron acceleration. *Journal of Geophysical Research: Space Physics*, *124*, 2628–2642. https://doi.org/10.1029/2019JA026516

Allison, H. J., Shprits, Y. Y., Zhelavskaya, I. S., Wang, D., & Smirnov, A. G. (2021). Gyroresonant wave-particle interactions with chorus waves during extreme depletions of plasma density in the Van Allen radiation belts. *Science Advances*, *7*(5), eabc0380. https://doi.org/10.1126/sciadv.abc0380

Baker, D. N. (1998). What is space weather? *Advances in Space Researc*h, *22*(1), 7–16. https://doi.org/10.1016/S0273-1177(97)01095-8

Baker, D. N. (2001). Satellite anomalies due to space storms. In I. A. Daglis (Ed.), *Space storms and space weather hazards*, *NATO Science Series (Series II: Mathematics, Physics and Chemistry)* (Vol. 38, pp. 285–311). Springer.

Baker, D. N., Allen, J. H., Kanekal, S. G., & Reeves, G. D. (1998). Disturbed space environment may have been related to pager satellite failure. *Eos, Transactions American Geophysical Union*, *79*(40), 477–483. https://doi.org/10.1029/98EO00359

Baker, D. N., Hoxie, V., Zhao, H., Jaynes, A. N., Kanekal, S., Li, X., & Elkington, S. (2019). Multiyear measurements of radiation belt electrons: Acceleration, transport, and loss. *Journal of Geophysical Research: Space Physics*, *124*(4), 2588–2602. https://doi.org/10.1029/2018JA026259

Baker, D. N., Kanekal, S. G., Hoxie, V., Li, X., Jaynes, A. N., Zhao, H., et al. (2021). The Relativistic Electron-Proton Telescope (REPT) investigation: Design, operational properties, and science highlights. *Space Science Reviews*, *217*(5), 68. https://doi.org/10.1007/s11214-021-00838-3

Baker, D. N., Kanekal, S. G., Hoxie, V. C., Batiste, S., Bolton, M., Li, X., et al. (2013). The Relativistic Electron-Proton Telescope (REPT) instrument on board the Radiation Belt Storm Probes (RBSP) spacecraft: Characterization of Earth's radiation belt high-energy particle populations. *Space Science Reviews*, *179*(1–4), 337–381. https://doi.org/10.1007/s11214-012-9950-9

Baker, D. N., Kanekal, S. G., Li, X., Monk, S. P., Goldstein, J., & Burch, J. L. (2004). An extreme distortion of the Van Allen belt arising from the 'Hallowe'en' solar storm in 2003. *Nature*, *432*(7019), 878–881. https://doi.org/10.1038/nature03116

Berner, J., Ha, S. Y., Hacker, J. P., Fournier, A., & Snyder, C. (2011). Model uncertainty in a mesoscale ensemble prediction system: Stochastic versus multiphysics representations. *Monthly Weather Review*, *139*(6), 1972–1995. https://doi.org/10.1175/2010MWR3595.1

Blake, J. B., Carranza, P. A., Claudepierre, S. G., Clemmons, J. H., Crain, W. R., Dotan, Y., et al. (2013). The Magnetic Electron Ion Spectrometer (MagEIS) instruments aboard the Radiation Belt Storm Probe (RBSP) spacecraft. *Space Science Reviews*, *179*(1–4), 383–421. https://doi.org/10.1007/s11214-013-9991-8

Bortnik, J., Ma, Q., Chu, X., Li, W., Claudepierre, S. G., Ni, B., & Angelopoulos, V. (2019). The use of machine learning for the rapid prediction of radiation belt dynamics. *Paper presented at American Geophysical Union, Fall Meeting 2019, San Francisco, CA, U.S.* Retrieved from https://ui.adsabs.harvard.edu/%23abs/2019AGUFMSM52A.02B/abstract

Bortnik, J., Thorne, R. M., & Inan, U. S. (2008). Nonlinear interaction of energetic electrons with large amplitude chorus. *Geophysical Research Letters*, *35*(21), L21102. https://doi.org/10.1029/2008GL035500

Camporeale, E., Shprits, Y., Chandorkar, M., Drozdov, A., & Wing, S. (2016). On the propagation of uncertainties in radiation belt simulations. *Space Weather*, *14*(11), 982–992. https://doi.org/10.1002/2016SW001494

Cash, M. D., Biesecker, D. A., Pizzo, V., de Koning, C. A., Millward, G., Arge, C. N., et al. (2015). Ensemble modeling of the 23 July 2012 coronal mass ejection. *Space Weather*, *13*(10), 611–625. https://doi.org/10.1002/2015SW001232

Chen, M. W., O'Brien, T. P., Lemon, C. L., & Guild, T. B. (2018). Effects of uncertainties in electric field boundary conditions for ring current simulations. *Journal of Geophysical Research: Space Physics*, *123*(1), 638–652. https://doi.org/10.1002/2017JA024496

Claudepierre, S. G., Blake, J. B., Boyd, A. J., Clemmons, J. H., Fennell, J. F., Gabrielse, C., et al. (2021). The magnetic electron Ion spectrometer: A review of on-orbit sensor performance, data, operations, and science. *Space Science Reviews*, *217*(8), 80. https://doi.org/10.1007/s11214-021-00855-2

Claudepierre, S. G., Ma, Q., Bortnik, J., O'Brien, T. P., Fennell, J. F., & Blake, J. B. (2020). Empirically estimated electron lifetimes in the Earth's radiation belts: Comparison with theory. *Geophysical Research Letters*, *47*(3), e2019GL086056. https://doi.org/10.1029/2019GL086056

Drozdov, A. Y., Blum, L. W., Hartinger, M., Zhao, H., Lejosne, S., Hudson, M. K., et al. (2022). Radial transport versus local acceleration: The long-standing debate. *Earth and Space Science*, *9*(2), e2022EA002216. https://doi.org/10.1029/2022EA002216

Dumbović, M., Čalogović, J., Vrsnak, B., Temmer, M., Mays, M. L., Veronig, A., & Piantschitsch, I. (2018). The drag-based ensemble model (DBEM) for coronal mass ejection propagation. *The Astrophysical Journal*, *854*(2), 180. https://doi.org/10.3847/1538-4357/aaaa66

Gan, L., Li, W., Ma, Q., Albert, J. M., Artemyev, A. V., & Bortnik, J. (2020). Nonlinear interactions between radiation belt electrons and chorus waves: Dependence on wave amplitude modulation. *Geophysical Research Letters*, *47*(4), e2019GL085987. https://doi.org/10.1029/2019GL085987

Glauert, S. A., & Horne, R. B. (2005). Calculation of pitch angle and energy diffusion coefficients with the PADIE code. *Journal of Geophysical Research*, *110*(A4), A04206. https://doi.org/10.1029/2004JA010851

Green, J. C., & Kivelson, M. G. (2004). Relativistic electrons in the outer radiation belt: Differentiating between acceleration mechanisms. *Journal of Geophysical Research*, *109*(A3), A03213. https://doi.org/10.1029/2003JA010153

Greybush, S. J., Saslo, S., & Grumm, R. (2017). Assessing the ensemble predictability of precipitation forecasts for the January 2015 and 2016 East Coast winter storms. *Weather and Forecasting*, *32*(3), 1057–1078. https://doi.org/10.1175/WAF-D-16-0153.1

Guerra, J. A., Murray, S. A., & Doornbos, E. (2020). The use of ensembles in space weather forecasting. *Space Weather*, *18*(2), e2020SW002443. https://doi.org/10.1029/2020SW002443

Horne, R. B. (2007). Acceleration of killer electrons. *Nature Physics*, *3*(9), 590–591. https://doi.org/10.1038/nphys703

Horne, R. B., Kersten, T., Glauert, S. A., Meredith, N. P., Boscher, D., Sicard-Piet, A., et al. (2013). A new diffusion matrix for whistler mode chorus waves. *Journal of Geophysical Research: Space Physics*, *118*(10), 6302–6318. https://doi.org/10.1002/jgra.50594

Horne, R. B., Thorne, R. M., Glauert, S. A., Albert, J. M., Meredith, N. P., & Anderson, R. R. (2005). Timescale for radiation belt electron acceleration by whistler mode chorus waves. *Journal of Geophysical Research*, *110*(A3), A03225. https://doi.org/10.1029/2004JA010811

Hua, M., Bortnik, J., Kellerman, A. C., Camporeale, E., & Ma, Q. (2022). Ensemble modeling of radiation belt electron flux decay following a geomagnetic storm: Dependence on key input parameters. *Space Weather*, *20*(8), e2022SW003051. https://doi.org/10.1029/2022SW003051

Hua, M., Bortnik, J., Kellerman, A. C., Camporeale, E., & Ma, Q. (2023). Ensemble modeling of radiation belt electron acceleration by chorus waves: Dependence on key input parameters [Dataset]. figshare. https://doi.org/10.6084/m9.figshare.20321670.v1

Hua, M., Bortnik, J., & Ma, Q. (2022). Upper limit of outer radiation belt electron acceleration driven by whistler-mode chorus waves. *Geophysical Research Letters*, *49*(15), e2022GL099618. https://doi.org/10.1029/2022GL099618

Hua, M., Li, W., Ni, B., Ma, Q., Green, A., Shen, X.-C., et al. (2020). Very-low-frequency transmitters bifurcate energetic electron belt in near-earth space. *Nature Communications*, *11*(1), 4847. https://doi.org/10.1038/s41467-020-18545-y

Hua, M., Ni, B., Fu, S., Gu, X., Xiang, Z., Cao, X., et al. (2018). Combined scattering of outer radiation belt electrons by simultaneously occurring chorus, exohiss, and magnetosonic waves. *Geophysical Research Letters*, *45*(19), 10057–10067. https://doi.org/10.1029/2018GL079533

Hua, M., Ni, B., Li, W., Gu, X., Fu, S., Shi, R., et al. (2019). Evolution of radiation belt electron pitch angle distribution due to combined scattering by plasmaspheric hiss and magnetosonic waves. *Geophysical Research Letters*, *46*(6), 3033–3042. https://doi.org/10.1029/2018GL081828

Jaynes, A. N., Ali, A. F., Elkington, S. R., Malaspina, D. M., Baker, D. N., Li, X., et al. (2018). Fast diffusion of ultrarelativistic electrons in the outer radiation belt: 17 March 2015 storm event. *Geophysical Research Letters*, *45*(20), 10874–10882. https://doi.org/10.1029/2018GL079786

Kalnay, E. (2019). Historical perspective: Earlier ensembles and forecasting forecast skill. *Quarterly Journal of the Royal Meteorological Society*, *145*(S1), 25–34. https://doi.org/10.1002/qj.3595

Kletzing, C. A., Kurth, W. S., Acuna, M., MacDowall, R. J., Torbert, R. B., Averkamp, T., et al. (2013). The electric and magnetic field instrument suite and integrated science (EMFISIS) on RBSP. *Space Science Reviews*, *179*(1–4), 127–181. https://doi.org/10.1007/s11214-013-9993-6

Knipp, D. J. (2016). Advances in space weather ensemble forecasting. *Space Weather*, *14*(2), 52–53. https://doi.org/10.1002/2016SW001366

Krishnamurti, T. N., Kishtawal, C. M., Zhang, Z., LaRow, T., Bachiochi, D., Williford, E., et al. (2000). Multimodel ensemble forecasts for weather and seasonal climate. *Journal of Climate*, *13*(23), 4196–4216. https://doi.org/10.1175/1520-0442(2000)013<4196:MEFFWA>2.0.CO;2

Kurth, W. S., De Pascuale, S., Faden, J. B., Kletzing, C. A., Hospodarsky, G. B., Thaller, S., & Wygant, J. R. (2015). Electron densities inferred from plasma wave spectra obtained by the Waves instrument on Van Allen Probes. *Journal of Geophysical Research: Space Physics*, *120*(2), 904–914. https://doi.org/10.1002/2014JA020857

Lei, M., Xie, L., Li, J., Pu, Z., Fu, S., Ni, B., et al. (2017). The radiation belt electron scattering by magnetosonic wave: Dependence on key parameters. *Journal of Geophysical Research: Space Physics*, *122*(12), 12338–12352. https://doi.org/10.1002/2016JA023801

Li, L. Y., Yu, J., Cao, J. B., Yang, J. Y., Li, X., Baker, D. N., et al. (2017). Roles of whistler mode waves and magnetosonic waves in changing the outer radiation belt and the slot region. *Journal of Geophysical Research: Space Physics*, *122*(5), 5431–5448. https://doi.org/10.1002/2016JA023634

Li, W., & Hudson, M. K. (2019). Earth's Van Allen radiation belts: From discovery to the Van Allen Probes era. *Journal of Geophysical Research: Space Physics*, *124*(11), 8319–8351. https://doi.org/10.1029/2018JA025940

Li, W., Ma, Q., Thorne, R. M., Bortnik, J., Zhang, X. J., Li, J., et al. (2016). Radiation belt electron acceleration during the 17 March 2015 geomagnetic storm: Observations and simulations. *Journal of Geophysical Research: Space Physics*, *121*(6), 5520–5536. https://doi.org/10.1002/2016JA022400

Li, W., Santolik, O., Bortnik, J., Thorne, R. M., Kletzing, C. A., Kurth, W. S., & Hospodarsky, G. B. (2016). New chorus wave properties near the equator from Van Allen Probes wave observations. *Geophysical Research Letters*, *43*(10), 4725–4735. https://doi.org/10.1002/2016GL068780

Li, W., Thorne, R. M., Ma, Q., Ni, B., Bortnik, J., Baker, D. N., et al. (2014). Radiation belt electron acceleration by chorus waves during the 17 March 2013 storm. *Journal of Geophysical Research: Space Physics*, *119*(6), 4681–4693. https://doi.org/10.1002/2014JA019945

Loridan, V., Ripoll, J.-F., Tu, W., & Cunningham, G. S. (2019). On the use of different magnetic field models for simulating the dynamics of the outer radiation belt electrons during the October 1990 storm. *Journal of Geophysical Research: Space Physics*, *124*(8), 6453–6486. https://doi.org/10.1029/2018JA026392

Ma, Q., Li, W., Bortnik, J., Thorne, R. M., Chu, X., Ozeke, L. G., et al. (2018). Quantitative evaluation of radial diffusion and local acceleration processes during GEM challenge events. *Journal of Geophysical Research: Space Physics*, *123*(3), 1938–1952. https://doi.org/10.1002/2017JA025114

Ma, Q., Li, W., Thorne, R. M., Ni, B., Kletzing, C. A., Kurth, W. S., et al. (2015). Modeling inward diffusion and slow decay of energetic electrons in the Earth's outer radiation belt. *Geophysical Research Letters*, *42*(4), 987–995. https://doi.org/10.1002/2014GL062977

Ma, Q., Li, W., Thorne, R. M., Nishimura, Y., Zhang, X., Reeves, G. D., et al. (2016). Simulation of energy-dependent electron diffusion processes in the Earth's outer radiation belt. *Journal of Geophysical Research: Space Physics*, *121*(5), 4217–4231. https://doi.org/10.1002/2016JA022507

Ma, Q., Ni, B., Tao, X., & Thorne, R. M. (2012). Evolution of the plasma sheet electron pitch angle distribution by whistler-mode chorus waves in non-dipole magnetic fields. *Annals of Geophysics*, *30*(4), 751–760. https://doi.org/10.5194/angeo-30-751-2012

Mauk, B. H., Fox, N. J., Kanekal, S. G., Kessel, R. L., Sibeck, D. G., & Ukhorskiy, A. (2013). Science objectives and rationale for the radiation belt storm probes mission. *Space Science Reviews*, *179*(1–4), 3–27. https://doi.org/10.1007/s11214-012-9908-y

Mays, M. L., Taktakishvili, A., Pulkkinen, A., MacNeice, P. J., Rastatter, L., Odstrcil, D., et al. (2015). Ensemble modeling of CMEs using the WSA–ENLIL+Cone model. *Solar Physics*, *290*(6), 1775–1814. https://doi.org/10.1007/s11207-015-0692-1

Meredith, N. P., Horne, R. B., Shen, X.-C., Li, W., & Bortnik, J. (2020). Global model of whistler mode chorus in the near-equatorial region ($|\lambda m| < 18°$). *Geophysical Research Letters*, *47*(11), e2020GL087311. https://doi.org/10.1029/2020GL087311

Meredith, N. P., Horne, R. B., Sicard-Piet, A., Boscher, D., Yearby, K. H., Li, W., & Thorne, R. M. (2012). Global model of lower band and upper band chorus from multiple satellite observations. *Journal of Geophysical Research*, *117*(A10), A10225. https://doi.org/10.1029/2012JA017978

Migliorini, S., Dixon, M., Bannister, R., & Ballard, S. (2011). Ensemble prediction for nowcasting with a convection-permitting model—I: Description of the system and the impact of radar-derived surface precipitation rates. *Tellus Series A: Dynamic Meteorology and Oceanography*, *63*(3), 468–496. https://doi.org/10.1111/j.1600-0870.2010.00503.x

Morley, S. K. (2020). Challenges and opportunities in magnetospheric space weather prediction. *Space Weather*, *18*(3), e2018SW002108. https://doi.org/10.1029/2018SW002108

Morley, S. K., Sullivan, J. P., Henderson, M. G., Blake, J. B., & Baker, D. N. (2016). The Global Positioning System constellation as a space weather monitor: Comparison of electron measurements with Van Allen Probes data. *Space Weather*, *14*(2), 76–92. https://doi.org/10.1002/2015SW001339

Morley, S. K., Welling, D. T., & Woodroffe, J. R. (2018). Perturbed input ensemble modeling with the space weather modeling framework. *Space Weather*, *16*(9), 1330–1347. https://doi.org/10.1029/2018SW002000

Mourenas, D., Zhang, X.-J., Artemyev, A. V., Angelopoulos, V., Thorne, R. M., Bortnik, J., et al. (2018). Electron nonlinear resonant interaction with short and intense parallel chorus wave packets. *Journal of Geophysical Research: Space Physics*, *123*(6), 4979–4999. https://doi.org/10.1029/2018JA025417

Mourenas, D., Zhang, X.-J., Nunn, D., Artemyev, A. V., Angelopoulos, V., Tsai, E., & Wilkins, C. (2022). Short chorus wave packets: Generation within chorus elements, statistics, and consequences on energetic electron precipitation. *Journal of Geophysical Research: Space Physics*, *127*(5), e2022JA030310. https://doi.org/10.1029/2022JA030310

Murray, S. A. (2018). The importance of ensemble techniques for operational space weather forecasting. *Space Weather*, *16*(7), 777–783. https://doi.org/10.1029/2018SW001861

Ni, B., Bortnik, J., Nishimura, Y., Thorne, R. M., Li, W., Angelopoulos, V., et al. (2014). Chorus wave scattering responsible for the Earth's dayside diffuse auroral precipitation: A detailed case study. *Journal of Geophysical Research: Space Physics*, *119*(2), 897–908. https://doi.org/10.1002/2013JA019507

Ni, B., Hua, M., Zhou, R., Yi, J., & Fu, S. (2017). Competition between outer zone electron scattering by plasmaspheric hiss and magnetosonic waves. *Geophysical Research Letters*, *44*(8), 3465–3474. https://doi.org/10.1002/2017GL072989

Ni, B., Thorne, R. M., & Ma, Q. (2012). Bounce-averaged Fokker-Planck diffusion equation in non-dipolar magnetic fields with applications to the Dungey magnetosphere. *Annals of Geophysics*, *30*(4), 733–750. https://doi.org/10.5194/angeo-30-733-2012

Orlova, K. G., Shprits, Y. Y., & Ni, B. (2012). Bounce-averaged diffusion coefficients due to resonant interaction of the outer radiation belt electrons with oblique chorus waves computed in a realistic magnetic field model. *Journal of Geophysical Research*, *117*(A7), A07209. https://doi.org/10.1029/2012JA017591

Ozeke, L. G., Mann, I. R., Dufresne, S. K. Y., Olifer, L., Morley, S. K., Claudepierre, S. G., et al. (2020). Rapid outer radiation belt flux dropouts and fast acceleration during the March 2015 and 2013 storms: The role of ULF wave transport from a dynamic outer boundary. *Journal of Geophysical Research: Space Physics*, *125*(2), e2019JA027179. https://doi.org/10.1029/2019JA027179

Reeves, G. D., Friedel, R. H. W., Larsen, B. A., Skoug, R. M., Funsten, H. O., Claudepierre, S. G., et al. (2016). Energy-dependent dynamics of keV to MeV electrons in the inner zone, outer zone, and slot regions. *Journal of Geophysical Research: Space Physics*, *121*(1), 397–412. https://doi.org/10.1002/2015JA021569

Reeves, G. D., Spence, H. E., Henderson, M. G., Morley, S. K., Friedel, R. H. W., Funsten, H. O., et al. (2013). Electron acceleration in the heart of the Van Allen radiation belts. *Science*, *341*(6149), 991–994. https://doi.org/10.1126/science.1237743

Ripoll, J.-F., Claudepierre, S. G., Ukhorskiy, A. Y., Colpitts, C., Li, X., Fennell, J., & Crabtree, C. (2020). Particle dynamics in the Earth's radiation belts: Review of current research and open questions. *Journal of Geophysical Research: Space Physics*, *125*(5), e2019JA026735. https://doi.org/10.1029/2019JA026735

Ripoll, J.-F., Loridan, V., Denton, M. H., Cunningham, G., Reeves, G., Santolík, O., et al. (2019). Observations and Fokker-Planck simulations of the L-shell, energy, and pitch angle structure of Earth's electron radiation belts during quiet times. *Journal of Geophysical Research: Space Physics*, *124*, 1125–1142. https://doi.org/10.1029/2018JA026111

Ripoll, J.-F., Reeves, G. D., Cunningham, G. S., Loridan, V., Denton, M., Santolík, O., et al. (2016). Reproducing the observed energy-dependent structure of Earth's electron radiation belts during storm recovery with an event-specific diffusion model. *Geophysical Research Letters*, *43*(11), 5616–5625. https://doi.org/10.1002/2016GL068869

Ripoll, J.-F., Santolík, O., Reeves, G. D., Kurth, W. S., Denton, M. H., Loridan, V., et al. (2017). Effects of whistler mode hiss waves in March 2013. *Journal of Geophysical Research: Space Physics*, *122*(2), 7433–7462. https://doi.org/10.1002/2017JA024139

Ross, J. P. J., Glauert, S. A., Horne, R. B., Watt, C. E., Meredith, N. P., & Woodfield, E. E. (2020). A new approach to constructing models of electron diffusion by EMIC waves in the radiation belts. *Geophysical Research Letters*, *47*(20), e2020GL088976. https://doi.org/10.1029/2020GL088976

Sarma, R., Chandorkar, M., Zhelavskaya, I., Shprits, Y., Drozdov, A., & Camporeale, E. (2020). Bayesian inference of quasi-linear radial diffusion parameters using Van Allen Probes. *Journal of Geophysical Research: Space Physics*, *125*(5), e2019JA027618. https://doi.org/10.1029/2019JA027618

Schunk, R. W., Scherliess, L., Eccles, V., Gardner, L. C., Sojka, J. J., Zhu, L., et al. (2014). Ensemble modeling with data assimilation models: A new strategy for space weather specifications, forecasts, and science. *Space Weather*, *12*(3), 123–126. https://doi.org/10.1002/2014SW001050

Schunk, R. W., Scherliess, L., Eccles, V., Gardner, L. C., Sojka, J. J., Zhu, L., et al. (2016). Space weather forecasting with a Multimodel Ensemble Prediction System (MEPS). *Radio Science*, *51*(7), 1157–1165. https://doi.org/10.1002/2015RS005888

Sheeley, B. W., Moldwin, M. B., Rassoul, H. K., & Anderson, R. R. (2001). An empirical plasmasphere and trough density model: CRRES observations. *Journal of Geophysical Research*, *106*(A11), 25631–25641. https://doi.org/10.1029/2000JA000286

Spence, H. E., Reeves, G. D., Baker, D. N., Blake, J. B., Bolton, M., Bourdarie, S., et al. (2013). Science goals and overview of the radiation belt storm probes (RBSP) energetic particle, composition, and thermal plasma (ECT) suite on NASA's Van Allen Probes mission. *Space Science Reviews*, *179*(1–4), 311–336. https://doi.org/10.1007/s11214-013-0007-5

Storer, L. N., Gill, P. G., & Williams, P. D. (2019). Multi-model ensemble predictions of aviation turbulence. *Meteorological Applications*, *26*(3), 416–428. https://doi.org/10.1002/met.1772

Summers, D., Mann, I. R., & Baker, D. N. (2011). State of the art in radiation belt research. *Eos, Transactions American Geophysical Union*, *92*(49), 457. https://doi.org/10.1029/2011eo490011

Tao, X., Bortnik, J., Albert, J. M., & Thorne, R. M. (2012). Comparison of bounce-averaged quasi-linear diffusion coefficients for parallel propagating whistler mode waves with test particle simulations. *Journal of Geophysical Research*, *117*(A10), A10205. https://doi.org/10.1029/2012JA017931

Thompson, R. L., Watt, C. E. J., & Williams, P. D. (2020). Accounting for variability in ULF wave radial diffusion models. *Journal of Geophysical Research: Space Physics*, *125*(8), e2019JA027254. https://doi.org/10.1029/2019JA027254

Thorne, R. M., Li, W., Ni, B., Ma, Q., Bortnik, J., Chen, L., et al. (2013). Rapid local acceleration of relativistic radiation-belt electrons by magnetospheric chorus. *Nature*, *504*(7480), 411–414. https://doi.org/10.1038/nature12889

Tsyganenko, N. A., Singer, H. J., & Kasper, J. C. (2003). Storm-time distortion of the inner magnetosphere: How severe can it get? *Journal of Geophysical Research*, *108*, 1209. https://doi.org/10.1029/2002JA009808

Tsyganenko, N. A., & Sitnov, M. I. (2005). Modeling the dynamics of the inner magnetosphere during strong geomagnetic storms. *Journal of Geophysical Research*, *110*(A3), A03208. https://doi.org/10.1029/2004JA010798

Tu, W., Cunningham, G. S., Chen, Y., Morley, S. K., Reeves, G. D., Blake, J. B., et al. (2014). Event-specific chorus wave and electron seed population models in DREAM3D using the Van Allen Probes. *Geophysical Research Letters*, *41*(5), 1359–1366. https://doi.org/10.1002/2013GL058819

Tu, W., Li, W., Albert, J. M., & Morley, S. K. (2019). Quantitative assessment of radiation belt modeling. *Journal of Geophysical Research: Space Physics*, *124*(2), 898–904. https://doi.org/10.1029/2018JA026414

Turner, D. L., Angelopoulos, V., Li, W., Bortnik, J., Ni, B., Ma, Q., et al. (2014). Competing source and loss mechanisms due to wave-particle interactions in Earth's outer radiation belt during the 30 September to 3 October 2012 geomagnetic storm. *Journal of Geophysical Research: Space Physics*, *119*, 1960–1979. https://doi.org/10.1002/2014JA019770

Turner, D. L., Angelopoulos, V., Li, W., Hartinger, M. D., Usanova, M., Mann, I. R., et al. (2013). On the storm-time evolution of relativistic electron phase space density in Earth's outer radiation belt. *Journal of Geophysical Research: Space Physics*, *118*(5), 2196–2212. https://doi.org/10.1002/jgra.50151

Varotsou, A., Boscher, D., Bourdarie, S., Horne, R. B., Meredith, N. P., Glauert, S. A., & Friedel, R. H. (2008). Three-dimensional test simulations of the outer radiation belt electron dynamics including electron-chorus resonant interactions. *Journal of Geophysical Research*, *113*(A12), A12212. https://doi.org/10.1029/2007JA012862

Wang, C., Ma, Q., Tao, X., Zhang, Y., Teng, S., Albert, J. M., et al. (2017). Modeling radiation belt dynamics using a 3-D layer method code. *Journal of Geophysical Research: Space Physics*, *122*(8), 8642–8658. https://doi.org/10.1002/2017JA024143

Wang, D., & Shprits, Y. Y. (2019). On how high-latitude chorus waves tip the balance between acceleration and loss of relativistic electrons. *Geophysical Research Letters*, *46*(14), 7945–7954. https://doi.org/10.1029/2019GL082681

Wang, D., Shprits, Y. Y., Zhelavskaya, I. S., Agapitov, O. V., Drozdov, A. Y., & Aseev, N. A. (2019). Analytical chorus wave model derived from Van Allen Probe observations. *Journal of Geophysical Research: Space Physics*, *124*(2), 1063–1084. https://doi.org/10.1029/2018JA026183

Watt, C. E. J., Allison, H. J., Meredith, N. P., Thompson, R. L., Bentley, S. N., Rae, I. J., et al. (2019). Variability of quasilinear diffusion coefficients for plasmaspheric hiss. *Journal of Geophysical Research: Space Physics*, *124*(11), 8488–8506. https://doi.org/10.1029/2018JA026401

Watt, C. E. J., Allison, H. J., Thompson, R. L., Bentley, S. N., Meredith, N. P., Glauert, S. A., et al. (2021). The implications of temporal variability in wave-particle interactions in Earth's radiation belts. *Geophysical Research Letters*, *48*(1), e2020GL089962. https://doi.org/10.1029/2020GL089962

Xiao, F., Su, Z., Zheng, H., & Wang, S. (2009). Modeling of outer radiation belt electrons by multidimensional diffusion process. *Journal of Geophysical Research*, *114*(A3), A03201. https://doi.org/10.1029/2008JA013580

Xiao, F., Yang, C., He, Z., Su, Z., Zhou, Q., He, Y., et al. (2014). Chorus acceleration of radiation belt relativistic electrons during March 2013 geomagnetic storm. *Journal of Geophysical Research: Space Physics*, *119*(5), 3325–3332. https://doi.org/10.1002/2014JA019822

Zhang, X.-J., Thorne, R., Artemyev, A., Mourenas, D., Angelopoulos, V., Bortnik, J., et al. (2018). Properties of intense field-aligned lower-band chorus waves: Implications for nonlinear wave-particle interactions. *Journal of Geophysical Research: Space Physics*, *123*(7), 5379–5393. https://doi.org/10.1029/2018JA025390

Zhao, H., Baker, D. N., Li, X., Jaynes, A. N., & Kanekal, S. G. (2018). The acceleration of ultrarelativistic electrons during a small to moderate storm of 21 April 2017. *Geophysical Research Letters*, *45*(12), 5818–5825. https://doi.org/10.1029/2018GL078582

Zhao, H., Baker, D. N., Li, X., Malaspina, D. M., Jaynes, A. N., & Kanekal, S. G. (2019). On the acceleration mechanism of ultrarelativistic electrons in the center of the outer radiation belt: A statistical study. *Journal of Geophysical Research: Space Physics*, *124*(11), 8590–8599. https://doi.org/10.1029/2019JA027111

Zhu, H., Shprits, Y. Y., Spasojevic, M., & Drozdov, A. Y. (2019). New hiss and chorus waves diffusion coefficient parameterizations from the Van Allen Probes and their effect on long-term relativistic electron radiation-belt verb simulations. *Journal of Atmospheric and Solar-Terrestrial Physics*, *193*, 105090. https://doi.org/10.1016/j.jastp.2019.105090

Zhu, Q., Cao, X., Gu, X., Ni, B., Xiang, Z., Fu, S., et al. (2021). Empirical loss timescales of slot region electrons due to plasmaspheric hiss based on Van Allen Probes observations. *Journal of Geophysical Research: Space Physics*, *126*(4), e2020JA029057. https://doi.org/10.1029/2020JA029057

References From the Supporting Information

Gelman, A., Carlin, J. B., Stern, H. S., & Rubin, D. B. (2004). *Bayesian data analysis* (2nd ed.). Chapman and Hall/CRC.